RESEARCH

Two New Sub-GLEs Found in Data of Neutron Monitors at South Pole and Vostok: On 09 June 1968 and 27 February 1969

Stepan Poluianov[1,2] · Oscar Batalla[3] · Alexander Mishev[1,2] · Sergey Koldobskiy[1,2] · Ilya Usoskin[1,2]

Abstract

Intense solar energetic particle (SEP) events can be observed by neutron monitors (NMs) as so-called ground-level enhancements (GLEs). High-altitude polar NMs have high sensitivity for SEP due to the reduced atmospheric energy cutoff and very low geomagnetic rigidity cutoff compared to other NMs. There is a special class of sub-GLE events, viz. events that are weaker than standard GLEs and can only be observed by high-altitude polar NMs. So far, only one sub-GLE and three candidates are known, all in the period 2012–2015. In this work, we inspected the period from March 1964 to December 1969 in the data of the South Pole and Vostok high-altitude polar NMs on the Antarctic Plateau in search of possible sub-GLEs. We found two previously unknown events from 09 June 1968 and 27 February 1969 that formally match the definition of sub-GLE. They were associated with significant enhancements in the integral SEP intensity $J(> 60 \text{ MeV})$ measured by space-borne particle detectors, as well as with strong X-class solar flares from the western part of the solar disk. The identified sub-GLEs were analyzed and the corresponding SEP characteristics were estimated.

Keywords Neutron monitor · Solar energetic particles · SEP · Ground-level enhancement · GLE · Sub-GLE

1. Introduction

Our Sun occasionally produces eruptive events, viz. flares and coronal mass ejections (CMEs), which can accelerate ions, mostly protons but also heavier species, and electrons, collectively known as solar energetic particles (SEPs), whose enhanced fluxes can be observed near Earth for hours or even days (e.g., Desai and Giacalone, 2016; Reames, 2017).

✉ S. Poluianov
    stepan.poluianov@oulu.fi

1   Sodankylä Geophysical Observatory, University of Oulu, 90014 Oulu, Finland

2   Space Physics and Astronomy Research Unit, University of Oulu, 90014 Oulu, Finland

3   Institute of Geophysics, National Autonomous University of Mexico, Investigación Científica C.U., Coyoacán, 04510, Mexico City, Mexico

🍃 Springer

High-energy SEPs can be accelerated by both solar flares (leading to so-called impulsive events) and CME-driven shocks (gradual events – see, e.g., Kocharov et al., 2018; Anastasiadis et al., 2019, and references therein).

Some strong SEP storms with high particle intensity can cause increases in the count rate of ground-based cosmic ray detectors, e.g., neutron monitors (NMs). Such events are called ground-level enhancements (GLEs), and their magnitudes range from a fraction to hundreds of percents of the background count rate, set by the omnipresent flux of galactic cosmic rays (GCRs). The enhancements provide very valuable information about the higher-energy part of the SEP spectrum. However, not every SEP storm can cause a GLE on Earth. Observation of a GLE depends on many SEP parameters, such as the geometry of particle propagation in the heliosphere, intensity, spectral hardness, and angular distribution.

SEP events were defined by the National Oceanic and Atmospheric Administration (NOAA) and United States Air Force (USAF) Space Environment Services Center in Boulder, Colorado, USA in 1976 as events with the proton intensity $J(> 10 \text{ MeV}) > 10$ particles $\text{cm}^{-2} \text{ sr}^{-1} \text{ s}^{-1}$ (Bazilevskaya et al., 2014). GLEs caused by strong SEP events are defined as an observation of a statistically significant increase in the count rate of at least two differently located near sea-level NMs, complemented by an independent observation by space- and/or balloon-borne instruments, implying significantly enhanced particle flux over the background (Poluianov et al., 2017).

Among the plethora of stations of the global NM network, there are featured high-altitude polar NMs. They have enhanced sensitivity to lower-energy cosmic rays, particularly to SEPs, vs. the sea-level NMs thanks to their reduced atmospheric cutoff due to their elevation (Mishev and Poluianov, 2021; Poluianov and Batalla, 2022) and negligibly low geomagnetic cutoff as a result of the proximity to the magnetic pole. Operation of such stations led to a need of revision of the definition of the GLE event (Poluianov et al., 2017) to keep the historical list of GLEs and modern observations of SEP homogeneous.

SEP events that cause enhancements of the count rate of only high-altitude polar NM stations and no statistically significant response from near-sea-level ones form a special class of SEP events called "sub-GLEs". Those events are formally defined as the following (Poluianov et al., 2017):

> A sub-GLE event is registered when there are near-time coincident and statistically significant enhancements of the count rates of at least two differently located high-elevation neutron monitors and a corresponding enhancement in the proton flux measured by a space-borne instrument(s), but no statistically significant enhancement in the count rates of neutron monitors near sea level.

The global NM network has had three high-altitude polar NM stations throughout its history. The most notable one is South Pole (the conventional acronym is SOPO), later accompanied by a lead-free (also called "bare") NM named SOPB, which has a different sensitivity and efficiency. It started working in 1964 and, although with breaks, continues its measurements to date. For many decades, it was the only high-altitude polar NM in the world. In 2015, the network was complemented with a pair of high-altitude polar NMs called DOMC (standard design) and DOMB (lead-free) installed at the research station Concordia at Dome C with the elevation of 3233 m above sea level (asl), also on the Antarctic Plateau (Poluianov et al., 2015), thanks to the hospitality program of the Italian Polar Research Program (PNRA). So far, only one sub-GLE is known, which occurred on 29 October 2015 and was registered by both SOPO/SOPB and DOMC/DOMB neutron monitors along with three more sub-GLE candidates detected by only SOPO/SOPB (i.e., no second NM station to confirm the events) on 27 January 2012, 07 March 2012, and 06 January 2014 (Mishev, Poluianov, and Usoskin, 2017, https://gle.oulu.fi).

There was also a period in the mid-1960s – early 1970s, when another high-altitude polar NM Vostok (VSTK) was in operation along with SOPO, but this data was not analyzed for signatures of possible sub-GLEs. VSTK was located at the Soviet research station Vostok, also on the Antarctic Plateau with the elevation of 3488 m asl. The simultaneous operation of these two high-altitude polar NMs over several years allows us to look for more sub-GLE events.

The search for unknown sub-GLEs is important because they complement and, with reservations, expand the list of GLEs, providing additional data for statistical analysis of SEP events with a high-energy component able to cause a response from ground-based neutron monitors. The current GLE list consists of 73 events, and every additional entry is very valuable.

In this work, we investigate the period of parallel operation of SOPO and VSTK and show that there are two events that can be considered as sub-GLEs not known so far. We analyze them and present estimates of their SEP spectra.

2. Data

2.1. Neutron Monitors

To search for sub-GLEs, we used two groups of neutron monitors. The first consists of two high-altitude polar stations needed to define a statistically significant increase in NM count rates during a SEP event, while the second contains sea-level polar NMs necessary to confirm the lack of a signal corresponding to the event. As mentioned in the introduction, the only simultaneously operational high-altitude polar NMs during the studied period were SOPO and VSTK, both located in Antarctica. As sea-level polar stations, we selected THUL and MCMD in the northern and southern hemispheres, respectively. These four NMs (see Table 1) were used for the data survey, but they were also complemented by other nine NMs with low geomagnetic cutoff needed for final confirmations and analyzes. The locations of these stations are shown on the map in Figure 1 and the basic information about them is summarized in Table 1.

We note that polar NMs typically have narrow asymptotic acceptance cones and therefore possess better angular resolution than other stations, which results in increased sensitivity to smaller variations of SEP spectra and angular distributions and, accordingly, a more accurate assessments of the apparent source location (Bieber and Evenson, 1995; Mishev and Usoskin, 2020). This is particularly important for the analysis of sub-GLEs (for details see Mishev, Poluianov, and Usoskin, 2017).

SOPO (South Pole) is a neutron monitor installed at the research station Amundsen-Scott, which is located exactly at the South Pole in Antarctica. The site has the elevation of 2820 m asl and nearly zero geomagnetic cutoff rigidity. The instrument has been in operation since March 1964, though with some breaks and upgrades. Initially, it was an IGY NM-type, but was upgraded to a 3NM64-type in 1977. Detailed descriptions of the NM types IGY and NM64 can be found in Simpson, Fonger, and Treiman (1953) and Hatton and Carmichael (1964), respectively. SOPO, as well as MCMD and THUL, is operated by the Bartol Research Institute, the University of Delaware, USA.

VSTK (Vostok) was a neutron monitor located at the research station Vostok at the Antarctic plateau with the elevation of 3488 m asl and zero geomagnetic cutoff rigidity. It was in operation from January 1963 to December 1972. For most of its lifetime, VSTK was an IGY-type setup (called "12NM57" by the operator Pushkov Institute of Terrestrial
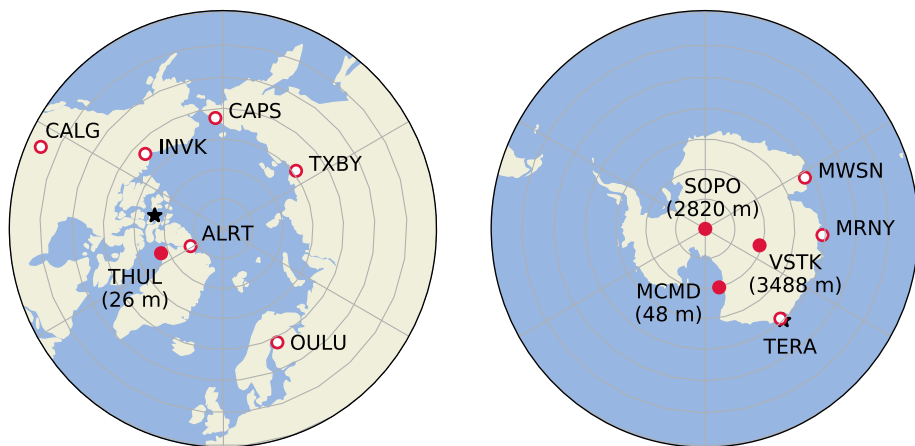
Figure 1 Maps of (sub)polar regions with indicated locations of the neutron monitors whose data were used in this work. The solid circles represent the stations used to search for sub-GLEs, while the open circles indicate the stations used to confirm the candidates. The numbers below some acronyms show the elevation in meters above sea level. The black stars indicate the locations of the magnetic poles in 1970. The coordinates and elevations are from nmdb.eu.

Table 1 Neutron monitors whose data were used in this work. The effective geomagnetic cutoff rigidity is denoted as R_c, its values were calculated in this work with the MAGNETOCOSMICS tool (Desorgher et al., 2005) for 09 June 1968 and 27 February 1969, see details in Section 4.1.

Name	Abbreviation	Elevation (m asl)	R_c (GV) 09 June 1968	R_c (GV) 27 February 1969
Used for searching sub-GLEs:				
South Pole	SOPO	2820	0.01	0.00
Vostok	VSTK	3488	0.00	0.00
McMurdo	MCMD	26	0.00	0.00
Thule	THUL	48	0.00	0.00
Used for confirmation:				
Alert	ALRT	57	0.00	0.00
Calgary	CALG	1128	0.92	0.84
Cape Schmidt	CAPS	0	0.31	0.20
Inuvik	INVK	0	0.03	0.01
Mirny	MRNY	30	0.00	0.00
Mawson	MWSN	30	0.26	0.14
Oulu	OULU	15	0.73	0.38
Terre Adelie	TERA	30	0.00	0.00
Tixie Bay	TXBY	0	0.29	0.08

Magnetism, Ionosphere and Radio Wave Propagation (IZMIRAN), USSR), but it was replaced with an instrument of the 6NM64 design, which provided data from January 1971 to the end of the operation in December 1972 (http://cr0.izmiran.ru/common/CR_detectors_IZMIRAN.pdf, in Russian).

THUL (Thule) is a neutron monitor located in Western Greenland (elevation 26 m asl, geomagnetic cutoff rigidity 0.0 GV). The instrument has been in operation since August 1957. Initially, it was the IGY NM-type and was upgraded to 9NM64 in October 1964.

Neutron monitor MCMD (McMurdo) was installed at the research station McMurdo at the coast of Antarctica with the elevation of 48 m asl and geomagnetic cutoff rigidity of 0.0 GV. It was working from May 1960 to January 2017 (https://nmdb.eu) with an upgrade from IGY to 18NM64 in February 1964.

Additionally, we used data of other high-latitude NMs along with the four mentioned stations for final checks and confirmations of the found sub-GLE candidates, as well as the comprehensive analysis of the findings (see details in Section 4.1). Those stations are ALRT, CALG, CAPS, INVK, MRNY, MWSN, OULU, TERA, and TXBY. Their properties are listed in Table 1 and the locations are shown in Figure 1.

The NM data are available at the World Data Center for Cosmic Rays hosted by the Nagoya University, Japan (https://cidas.isee.nagoya-u.ac.jp/WDCCR/index.html) and the IZMIRAN database (http://cr0.IZMIRAN.ru/common/links.htm). The data files in both sources have 1-hour resolution at best, they contain the count rate corrected for the atmospheric pressure (Väisänen, Usoskin, and Mursula, 2021). For this research, we used the IZMIRAN database.

Figure 2 shows the NM data availability over the studied period, as well as the sunspot number as an indicator for the phase of the solar cycle. In this work, we focused on the overlapping period of SOPO, VSTK, MCMD and THUL operations from March 1964 through December 1969, as defined by the start of the operation of SOPO and the end of the reliable operation of VSTK, see the pink areas in Figure 2. The period 1971 – 1972, when the mentioned NMs were also overlapping, was excluded from the analysis because the count rate of VSTK, once upgraded to a 3NM64, was in strong disagreement with SOPO, MCMD and THUL data (Figure 2). The studied period from March 1964 to December 1969 corresponds to the minimum, ascend and maximum phases of the Solar Cycle 20, when several GLEs #15 – 21 were registered by the global NM network (Miroshnichenko, 2015). We use one of those events, namely GLE #18 observed on 29 September 1968 by VSTK, SOPO, MCMD, THUL and shown in Figure 9 in the Appendix, as an example of a relatively weak ground-level enhancement.

2.2. Solar Energetic Particle Event Catalogues

For the search of sub-GLEs, SEP event catalogs were used in order to form the initial long list of events that can be potentially seen in the NM data. The most comprehensive data set was compiled by Dodson et al. (1975) for the period 1955 – 1969, but we complemented it with other extensive lists by McCracken, Rao, and Bukata (1967), Kinsey and McDonald (1968), King (1974), Reedy (1977), Shea et al. (1978), Shea and Smart (1990), Feynman et al. (1990), Bazilevskaya et al. (2010) and Barnard and Lockwood (2011). As a result, we obtained a long list, presented in Table 7 in the Appendix consisting of 38 strong SEP events that occurred in the studied period March 1964 – December 1969 and were reliably detected by riometers, balloon- and/or space-borne instruments.

2.3. Space-Borne Solar Energetic Particle Measurements

In addition to the catalogs, we used intensities of energetic protons directly measured by space-borne instruments. The data were compiled from different spacecraft, namely from Interplanetary Monitoring Platforms (IMP) 4 and 5, Anchored Interplanetary Monitoring
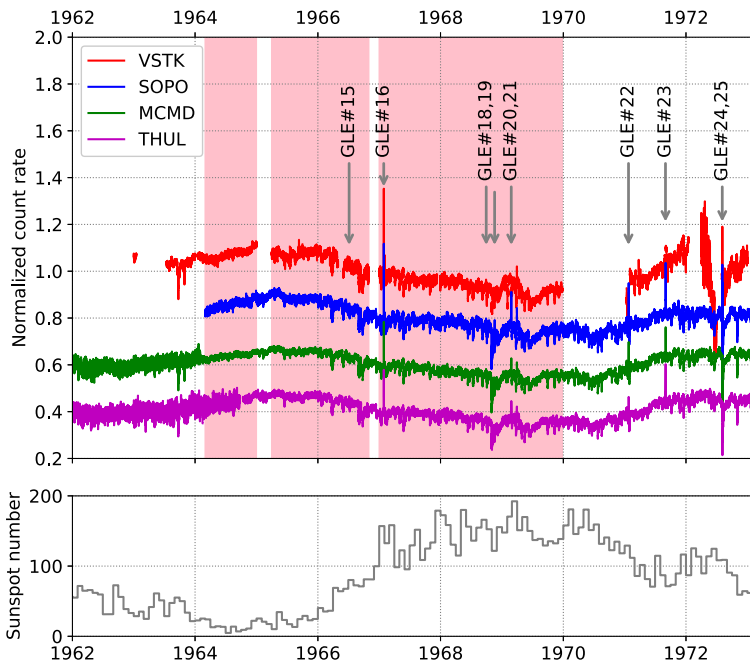
Figure 2 Normalized count rates of VSTK, SOPO, MCMD, and THUL neutron monitors used in this work (the top panel). The vertical arrows point to GLE events #15 – 25. Note that the count rates of SOPO, THUL and MCMD are shown with offsets for better display. The pink areas indicate the periods studied in this work, when all measurements are available. Monthly-mean sunspot number data are shown in the bottom panel as obtained from SILSO (https://www.sidc.be/silso/).

Platforms (AIMP) 1 and 2, Highly Eccentric Orbit Satellites (HEOS) 1 and 2. They are available in the database OMNI (Papitashvili and King, 2020, https://omniweb.gsfc.nasa.gov), where one can find the integral proton intensities $J(> 10$ MeV$)$, $J(> 30$ MeV$)$, and $J(> 60$ MeV$)$ with 1-hour resolution for the studied period from 1967 to 1969, as well as other data not relevant to this work. We used $J(> 30$ MeV$)$ and $J(> 60$ MeV$)$ as the highest-energy direct measurements available, but ignored $J(> 10$ MeV$)$ because the population of lowest-energy SEPs can show very different behavior compared to the higher-energy one. The coverage of $J(> E)$ in OMNI starts from 30 May 1967, leaving the period from March 1964 to May 1967 without the hourly data. However, some information on the peak flux and fluence of events before May 1967 is available in the SEP event catalogs mentioned above (e.g., Feynman et al., 1990).

2.4. Solar Flare Observations

To complement our data investigations of SEP events with information about solar flares, we used flare catalogs of ground-based observations of the Sun in the optical band Hα and of space-borne measurements by satellites SOLRAD (SOLar RADiation) in the soft X-ray band 1 – 8 Å. The dataset on solar flares observed in Hα was prepared by the USAF Solar Observing Optical Network and made available via the NOAA National Geophysical Data Center (https://www.ngdc.noaa.gov/stp/space-weather/solar-data/solar-features/solar-flares/h-alpha/). The X-ray flare data are prepared by the NOAA National Geophysical

Data Center and can be acquired from https://www.ngdc.noaa.gov/stp/space-weather/solar-data/solar-features/solar-flares/x-rays/solrad/. We also relied on the Solar Geophysical Data Reports provided by NOAA (https://www.ngdc.noaa.gov/stp/solar/sgd.html), which conveniently contain various information on the solar and space observations reported by ground-based observatories and space missions.

3. Search of Sub-GLE Events

3.1. Procedure

The algorithm of the sub-GLE search consists of the following steps:

i) Collection of the available data from high-altitude and (near) sea-level polar NM stations as listed in Table 1;

ii) Compilation of an initial long list of SEP events that could be candidates to GLEs/sub-GLEs based on the analysis of SEP event catalogs and proton intensity $J(> 60 \text{ MeV})$ measured by satellites;

iii) Examination of the neutron monitor data from SOPO, VSTK, MCMD, and THUL for increases in the count rates matching the times of SEP events from the long list and consecutive reduction of that list to a short one with promising events for a detailed analysis;

iv) Careful analysis of the events from the shortlist, their time profiles, solar flare and satellite information about their onsets, maxima and endings;

v) Final confirmation of the found candidates as sub-GLEs by checking the data from the extended list of high-latitude NMs (see Table 1).

The long list was formed by 38 SEP events. After its examination in the NM data, the reduced shortlist contained only nine candidates, which were then carefully investigated and discussed. Eventually, after being corroborated by exploring data from other NMs, only two events were accepted as sub-GLE on 09 June 1968 and 27 February 1969, at the maximum of Solar Cycle 20 (Figure 2). There was also another strong candidate on 03 December 1967, which was not included due to a 3-hour delay in the SOPO count rate enhancement relative to VSTK, which cannot be naturally explained.

3.2. Event on 09 June 1968

The SEP event on 09 June 1968 was observed by satellite AIMP-1 as an enhancement of the intensity of protons $J(> 60 \text{ MeV})$. The increase started at 09:35 UT, reached its maximum at about 12 UT and lasted for more than one day. The maximum hourly value of $J(> 60 \text{ MeV})$ was 6.13 cm^{-2} sr^{-1} s^{-1}. The details of observations of the event, as well as the timeline are summarized in Table 2.

High-altitude polar NMs SOPO and VSTK showed a simultaneous increase in count rate with the magnitude of +1.28% and +0.97% over the GCR background, respectively. The background was estimated following the standard procedure, viz. as the mean count rate during two hours before the hour in which the event occurred. The z-scores of the SOPO and VSTK increases were 10.0 and 4.0 standard deviations of the background count rate, respectively, and we consider them as statistically significant, i.e., above the threshold of three standard deviations. The onset at 10 UT matched the $J(> 60 \text{ MeV})$ time profile measured by space-borne measurements very well (Figure 3). Sea-level polar neutron monitors MCMD
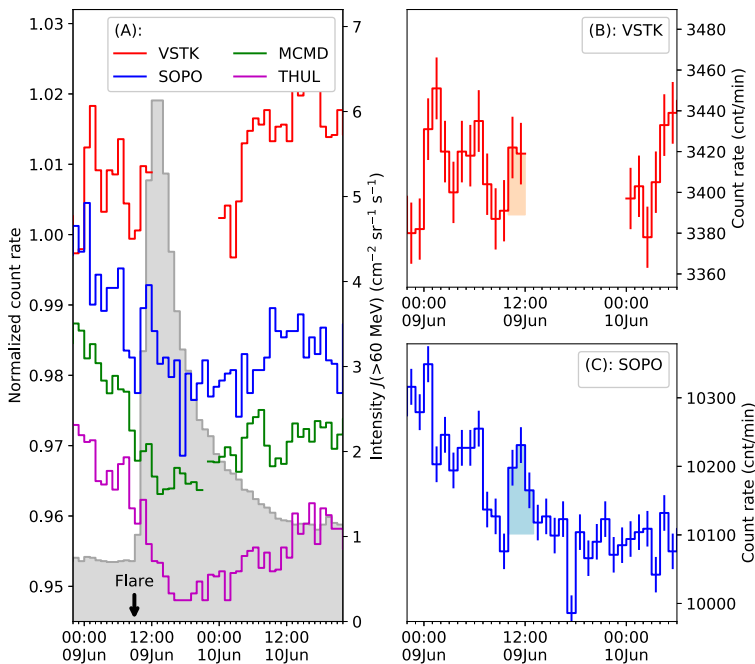
Figure 3 Sub-GLE on 09 June 1968 in the VSTK, SOPO, MCMD, and THUL neutron monitor count rates (lines) and proton intensity $J(> 60\,\text{MeV})$ from OMNI (gray shaded area). Panel (A): the NM count rates are shown normalized to the mean of two pre-event hours and with offsets for better visibility (0.00, −0.02, −0.03, −0.04 for VSTK, SOPO, MCMD, and THUL, respectively). The black arrow indicates the associated solar flare occurrence prior to the event. Panels (B) and (C): the count rates of VSTK and SOPO, respectively, in units of counts per minute. The shaded areas highlight the increased count rates over the background. The error bars correspond to the 95% confidence intervals (± 2 standard deviations, calculated as squared roots of the count rates).

and THUL also had very small, statistically insignificant increases of about +0.3%. We considered them as null responses of the instruments due to the lack of statistically significant responses. The other NMs listed in Section 2.1 neither had significant increases during this SEP event. The enhancement lasted for about 3 hours in the SOPO count rate (VSTK had a data gap from the third hour of the event) and the peak hourly value appeared between 11 and 12 UT.

Prior to the SEP event, a solar flare of 3B (3-Bright) importance with coordinates S13 W09 on the solar disk has been registered in Hα at 08:30 UT (Dodson et al., 1975). The satellite SOLRAD-8 observed the peak flux of 0.17 erg cm^{-2} s^{-1} = $1.7 \cdot 10^{-4}$ W m^{-2} in soft (1 − 8 Å) X-rays (SOLRAD database, NOAA). It can be translated to class X1.7, indicating that the flare was very strong.

3.3. Event on 27 February 1969

The SEP event on 27 February 1969 was observed as an increase in the proton intensity $J(> 60\,\text{MeV})$ with the onset at 15 UT, maximum at 19 UT, and end at about 20 UT on the next day, as seen in the left panel of Figure 4. The peak hourly-averaged intensity $J(> 60\,\text{MeV})$ measured by satellite IMP-4 was 4.35 cm^{-2} sr^{-1} s^{-1}. More details on the observations, including the timeline, are shown in Table 3.

Table 2 Observations accompanying the sub-GLE on 09 June 1968. The timeline of the event was compiled from Dodson et al. (1975), SOLRAD database (NOAA), OMNI, and the NM data.

Time (UT)	Observed features
08:30	Flare onset in Hα
08:38	Flare onset in soft X-rays
08:58	Flare maximum in soft X-rays
08:54	Flare maximum in Hα
09:35	Proton intensity $J(> 60\,\text{MeV})$ onset
10 – 11	NM count rate onset
>10:25	End of the flare in soft X-rays
10:30	End of the flare in Hα
11 – 12	Maximum increase in the NM count rate
12 – 13	Peak proton intensity $J(> 60\,\text{MeV})$
13 – 14	End of the event in the NM count rate

- 3B-importance flare observed in Hα at S14 W09 (Dodson et al., 1975)
- Peak soft X-ray flux of $1.7 \cdot 10^{-4}$ W m^{-2} measured by SOLRAD (NOAA)
- Maximum of 1-hour average intensity $J(> 60\,\text{MeV}) = 6.13$ cm^{-2} sr^{-1} s^{-1} (OMNI)
- Intensity ratio $J(> 60\,\text{MeV})/J(> 30\,\text{MeV}) = 0.52$ at the maximum (OMNI)
- Maximum count rate increases 1.28% and 0.97% in SOPO and VSTK, respectively

We found increases associated with this SEP signal in the neutron monitor data of SOPO and VSTK (Figure 4) with magnitudes of $+1.58\%$ and $+1.82\%$ over the GCR background, respectively. Those correspond to 12.1 (SOPO) and 8.1 (VSTK) standard deviations of the background count rates, notably above the statistical significance threshold of three standard deviations. The background count rate was calculated as the mean for two hours before the increase. The onset was between 17 and 18 UT and the maximum was registered between 18 and 19 UT. The overall duration was estimated as 4 hours. Other NMs used in this study (Section 2.1), including MCMD and THUL, show no or statistically insignificant responses.

This SEP event was associated with a solar flare that was first seen at 13:48 UT in the Hα line as 2B (2-Bright) at coordinates N13 W65 on the solar disk, and also had the onset of an increase in the $1 - 8$ Å soft X-ray flux registered by SOLRAD-9 at 13:56 UT (Dodson et al., 1975). The flare event ended at 15:05 UT and 16:00 UT in Hα and X-rays, respectively. The maximum soft X-ray intensity had a lower estimate of 0.50 erg cm^{-2} s^{-1} = $5.0 \cdot 10^{-4}$ W m^{-2} according to the SOLRAD data from NOAA, while the 14:00 – 15:00 UT average was reported as $284 \cdot 10^{-3}$ erg cm^{-2} s^{-1} = $2.84 \cdot 10^{-4}$ W m^{-2} (Environmental Science Services Administration, 1969, p. 98). This means that the flare of class X5.0 was very strong.

This sub-GLE is associated with the last SEP event in a dense sequence of events occurred in the end of February, including one on 25 February 1969 that caused GLE #20.

3.4. Possibility of Non-SEP Origins of the Events

The two newly found sub-GLEs have the count rate increases of $0.97 - 1.82\%$, which are slightly greater than the variations of the galactic cosmic ray background. Therefore, it is important to discuss whether the events have the SEP origin. The arguments supporting that origin are the following: (a) statistical significance of the NM count rate enhancements
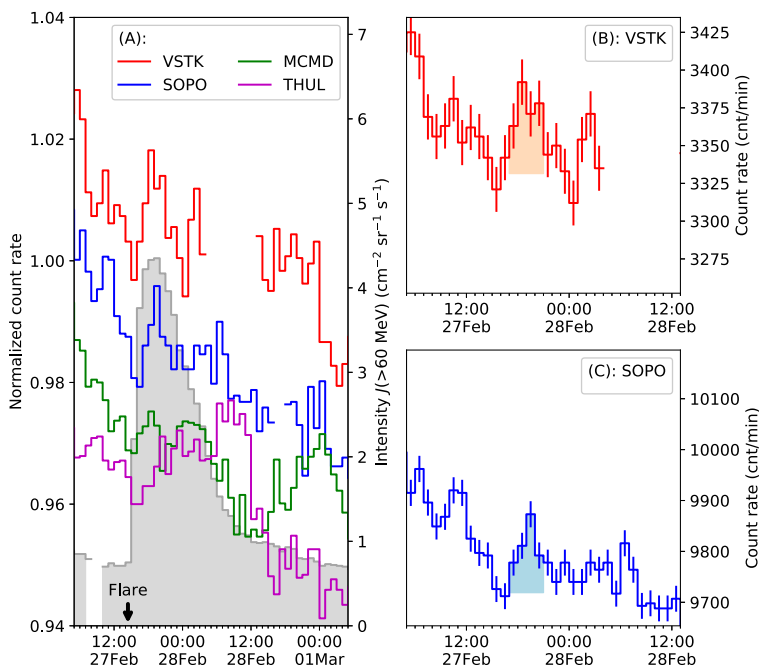
Figure 4 Sub-GLE on 27 February 1969 in the VSTK, SOPO, MCMD, and THUL neutron monitor count rates (lines) and proton intensity $J(> 60 \, \text{MeV})$ from OMNI (grey shaded area). Panel (A): the NM count rates are shown normalized to the mean of two pre-event hours and with offsets for better visibility (0.00, -0.02, -0.03, -0.04 for VSTK, SOPO, MCMD, and THUL, respectively). The black arrow indicates the associated solar flare occurrence prior the event. Panels (B) and (C): the count rates of VSTK and SOPO, respectively, in units of counts per minute. The shaded areas highlight the increased count rates over the background. The error bars correspond to the 95% confidence intervals (± 2 standard deviations, calculated as square roots of the count rates).

over the background; (b) agreement in timing of the observed increases in particle detectors onboard spacecraft and neutron monitors; (c) the hardness of SEP spectra observed with spacecraft implying the possible presence of high-energy particles with sufficient intensity to cause a detectable NM response. Strictly speaking, arguments (a) and (b) are formally sufficient to declare an NM increase as a sub-GLE, but we also paid attention to argument (c).

The SEP event on 09 June 1968 was recorded in the SOPO and VSTK data as statistically significant enhancements, with the onsets being slightly ahead of the proton intensity $J(> 60 \, \text{MeV})$ observed by a spacecraft, which is theoretically expected, since higher-energy SEPs causing an NM response usually arrive at Earth earlier than lower-energy particles because of the higher velocity. The ratio $J(> 60 \, \text{MeV})/J(> 30 \, \text{MeV})$, which indicates the hardness of the SEP spectrum, was 0.52 at the maximum intensity, which is close to a typical ratio for a relatively weak standard GLE (e.g., 0.61 for GLE #18, according to the OMNI database). On the other hand, the variability of the count rates prior to the event was comparable to the studied increase. However, the combination of the above factors leaves hardly any other explanation of the observed enhancement feasible than a sub-GLE.

The count rate increases observed with SOPO and VSTK during the event on 27 February 1969 were also statistically significant. However, the NM enhancement onsets were delayed with respect to proton intensity $J(> 60 \, \text{MeV})$ measured by a spacecraft by $1-2$ hours. The

Table 3 Observations accompanying the sub-GLE on 27 February 1969. The timeline of the event was compiled from Dodson et al. (1975), SOLRAD database (NOAA), OMNI, and the NM data.

Time (UT)	Observed features
13:48	Flare onset in Hα
13:56	Flare onset in soft X-rays
14:13	Flare maximum in Hα
14:14	Flare maximum in soft X-rays
15 – 16	Proton intensity $J(> 60\,\text{MeV})$ onset
15:05	End of the flare in Hα
16:00	End of the flare in soft X-rays
17 – 18	NM count rate onset
19 – 20	Peak in proton intensity $J(> 60\,\text{MeV})$, maximum increase in the NM count rate
21 – 22	End of the event in the NM count rate

- 2B-importance flare observed in Hα at N13 W65 (Dodson et al., 1975)
- Peak soft X-ray flux of $5.0 \cdot 10^{-4}\,\text{W m}^{-2}$ measured by SOLRAD-9 (NOAA)
- Maximum of 1-hour average intensity $J(> 60\,\text{MeV}) = 4.35\,\text{cm}^{-2}\,\text{sr}^{-1}\,\text{s}^{-1}$ (OMNI)
- Intensity ratio $J(> 60\,\text{MeV})/J(> 30\,\text{MeV}) = 0.44$ at the maximum (OMNI)
- Maximum count rate increases 1.58% and 1.82% in SOPO and VSTK, respectively

difference in onset times can be explained by the paradigm of two populations of SEPs. The flare-accelerated low energy SEPs were observed by a space probe as an impulsive event (prompt component), while the NM likely observed particles of the gradual events (delayed component) accelerated by an interplanetary shock (e.g., Reames, 1999; Moraal and Mc-Cracken, 2012). This plausible scenario is supported by the derived nearly anti-Sun arrival direction of SEPs during the event (Table 4, Figure 6) and Figure 8 (right panel), where two SEP populations are seen. The event on 27 February 1969 reveals a complex picture, most likely due to the series of previous eruptions at the Sun and complicated interplanetary transport of SEPs, the latter supported by the high value of the K_p index during the event onset ($K_p \approx 6$, see Table 8). However, a detailed analysis of the interplanetary conditions for this event is beyond the scope of this paper. Although a non-SEP origin for the observed increase on 27 February 1969 cannot be completely ruled out, it is unlikely and we consider it to be a sub-GLE.

4. Analysis of the Events

For the analysis of the events, we used two approaches, which we call the full and fast reconstructions of the SEP spectra. The former is an unfolding procedure based on the best-fit of the modelled NM responses on the given SEP spectrum into the experimental data (e.g., Mishev, Poluianov, and Usoskin, 2017), while the latter is based on the proportional scaling between the increase in NM count rate and integral fluence. The methods are cross-validated by Koldobskiy and Mishev (2022) and show a reasonably good agreement with direct PAMELA measurements (Bruno et al., 2018). Both approaches estimate the fluence (time- and energy/rigidity-integrated omnidirectional intensity) for each event. To complement the results in the lower energy range, we also used the OMNI database with data on the particle intensity from space-borne instruments to estimate fluence $F(> 30\,\text{MeV})$ and $F(> 60\,\text{MeV})$.

4.1. Full Reconstruction of the Intensity and Fluence

The full reconstruction method is based on the modelling of the global NM network response to the studied SEP event and corresponding optimization of the model parameters to fit the observed experimental NM count rate increases. The method is based on the approach originally proposed by Cramp et al. (1997). It involves computation of cut-off rigidities and asymptotic directions of the NMs used in the analysis and the least squares optimization (minimization) of the difference between experimental and modelled NM responses. Details and applications are given elsewhere (e.g., Mishev et al., 2018, 2022).

In general, the fit quality of the global NM network response is determined by the merit function

$$\mathcal{D} = \frac{\sqrt{\sum_{i=1}^{m}\left[\left(\frac{\Delta N_i}{N_i}\right)_{\text{mod}} - \left(\frac{\Delta N_i}{N_i}\right)_{\text{meas}}\right]^2}}{\sum_{i=1}^{m}(\frac{\Delta N_i}{N_i})_{\text{meas}}}, \tag{1}$$

where i indicates an NM in the data set consisting of m NMs in total, while $(\Delta N_i/N_i)_{\text{mod}}$ and $(\Delta N_i/N_i)_{\text{meas}}$ are the relative count rate increases of the i-th NM, modeled and measured, respectively.

We emphasize that $\mathcal{D}$ is typically $\leq 5\%$ for strong GLEs (e.g., see Vashenyuk et al., 2006), but it can be as high as $25-30\%$ for weak GLEs and sub-GLEs. The optimization is performed by the Levenberg–Marquardt (Levenberg, 1944; Marquardt, 1963) method using additional regularization (Aleksandrov, 1971; Golub and Van Loan, 1980; Mishev, Mavrodiev, and Stamenov, 2005), which allows one to select a reliable solution (for details see Tikhonov et al., 1995, and the discussion therein). We point out that the model should reproduce statistically significant count rate increases observed at some NM stations, as well as null responses of other NMs (for details see Cramp et al., 1997; Mishev et al., 2021, and the discussions therein). The latter is valuable for the determination of the boundary conditions for the SEP spectra and angular distributions and is specifically important for the sub-GLE analysis (for details see Mishev, Poluianov, and Usoskin, 2017).

Using NM records with removed galactic cosmic-ray background, we assessed the spectra and angular distributions of SEPs during the sub-GLE events considered in this study. The best-fit SEP spectra were achieved with a modified power-law function, where the analytical expression for the differential intensity of particles with rigidities $R > 1$ GV is

$$j_{\parallel}(R) = j_0 R^{-(\gamma + \delta\gamma(R-1\,\text{GV}))}. \tag{2}$$

Here, $j_{\parallel}(R)$ is the differential intensity (in particles cm^{-2} sr^{-1} s^{-1} GV^{-1}) of SEPs with rigidity R (in GV) along the axis of symmetry identified by the geographic latitude Ψ and longitude Λ, j_0 is the differential intensity (in particles cm^{-2} sr^{-1} s^{-1} GV^{-1}) at $R = 1$ GV, and γ is the power-law exponent (dimensionless) with the steepening of $\delta\gamma$ (in GV^{-1}).

This analysis allows us to take into account the anisotropy of particles. For that, the SEP angular distribution was approximated with a Gaussian function:

$$G(\alpha) \sim e^{-\alpha^2/\sigma^2}, \tag{3}$$

where α is the pitch angle (in radians) with respect to the direction of the magnetic field, and σ accounts for the width of the distribution, also in radians.

The computed asymptotic acceptance cones of NM stations used in the analysis are shown in Figures 5 and 6 for two sub-GLEs. They were calculated with a magnetospheric

Table 4 Best-fit spectral j_0, γ, $\delta\gamma$, and angular σ^2 distribution parameters of SEPs derived with the full method (see Section 4.1) and used in Equations 2–3. The values are presented with the 95% confidence intervals. Merit function $\mathcal{D}$ (Equation 1, range), latitudes Ψ and longitudes Λ of the anisotropy axis positions are also shown. The accuracy of Ψ and Λ is about ±12 degrees.

Interval (UT)	j_0 (cm^{-2} sr^{-1} s^{-1} GV^{-1})	γ	$\delta\gamma$ (GV^{-1})	σ^2 (rad^2)	Ψ (deg)	Λ (deg)	$\mathcal{D}$ (%)
sub-GLE on 09 June 1968							
10:00 – 11:00	$4.2^{+0.5}_{-0.2}$	$7.1^{+0.1}_{-0.1}$	1.9 ± 0.04	4.9 ± 0.1	5	−155	22 – 24
11:00 – 12:00	$4.6^{+0.5}_{-0.3}$	$7.3^{+0.2}_{-0.1}$	1.8 ± 0.05	5.2 ± 0.1	11	−161	21 – 23
12:00 – 13:00	$3.8^{+0.6}_{-0.2}$	$7.7^{+0.2}_{-0.1}$	1.8 ± 0.05	5.3 ± 0.2	12	−172	24 – 26
sub-GLE on 27 February 1969							
17:00 – 18:00	$4.7^{+0.4}_{-0.1}$	$6.8^{+0.02}_{-0.05}$	1.8 ± 0.03	3.7 ± 0.05	3	−144	26 – 28
18:00 – 19:00	$7.2^{+0.2}_{-0.1}$	$7.0^{+0.1}_{-0.05}$	1.7 ± 0.05	3.8 ± 0.1	8	−155	25 – 26
19:00 – 20:00	$6.5^{+0.2}_{-0.1}$	$7.1^{+0.1}_{-0.03}$	1.7 ± 0.05	4.1 ± 0.1	14	−168	20 – 22
20:00 – 21:00	$6.1^{+0.3}_{-0.1}$	$7.2^{+0.1}_{-0.05}$	1.7 ± 0.07	4.2 ± 0.1	17	−175	23 – 25

model as a superposition of the International Geomagnetic Reference Field (IGRF-13, Alken et al., 2021) and Tsyganenko-89 as the external field (Tsyganenko, 1989) using software MAGNETOCOSMICS (Desorgher et al., 2005). The used values of index K_{p}, which indicates disturbance of the outer magnetosphere, are shown in Table 8 in the Appendix. The approach provides a straightforward and reasonably accurate calculation of the charged-particle motion in the Earth's magnetic field (Kudela, Bučik, and Bobik, 2008; Nevalainen, Usoskin, and Mishev, 2013; Larsen, Mishev, and Usoskin, 2023). It was also used for computation of the geomagnetic cutoff rigidities of the NMs studied here (Table 1).

Accordingly, the illustrations of the derived differential particle intensities are given in the left-hand panels of Figures 7 and 8, while the details, including the best-fit parameters, are summarized in Table 4. One can see that the SEP spectra show moderate changes in the intensity and maintain approximately constant exponents γ during both events, which is typical for weak GLEs (e.g. Smart, Shea, and Gentile, 1994; Lovell et al., 2002), and accordingly plausible for sub-GLEs.

Using the reconstructed spectra evolving with the 1-hour time step, we calculated the particle fluence for each event with integration over pitch-angle α, rigidity R', and time t:

$$F(> E) = \int_{\text{event}} \left[2\pi \int_0^\pi G(\alpha, t) \sin\alpha \, d\alpha \cdot \int_{R(E)}^\infty j_\parallel(R', t) dR' \right] dt, \tag{4}$$

where $R(E) = \sqrt{E(E + 2E_0)}$ is the rigidity R corresponding to energy E for protons, and $E_0 = 0.938$ GeV is the proton's rest energy.

The 95% confidence intervals of $F(> E)$ from Equation 4 were estimated with the Monte Carlo approach and distribution of 10^4 fluence samples calculated from spectral parameters j_0, γ, $\delta\gamma$, and σ^2 randomly generated according to their best-fit values and corresponding uncertainties listed in Table 4.

The result fluences for the events on 09 June 1968 and 27 February 1969 are plotted in the right-hand panels of Figures 7 and 8, respectively. The tabulated values of the fluence for particle energies above 500, 700, and 1000 MeV are also shown in Table 6.
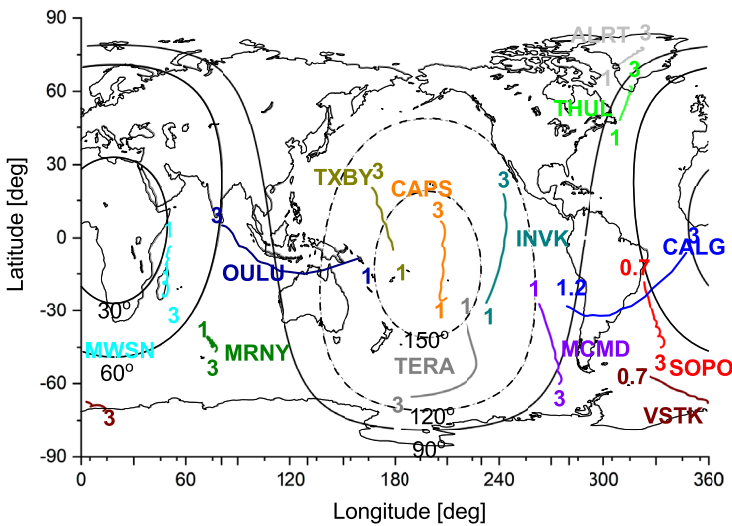
Figure 5 Asymptotic acceptance cones of selected polar NM stations during the sub-GLE on 09 June 1968 at 10:00 UT, shown in geographic coordinates. The cones are indicated as colored lines with NM names next to them and numbers showing the rigidities of SEP (in GV). The contour lines of equal particle pitch angles relative to the derived anisotropy axis are plotted for 30° and 60° for the sunward direction (black solid lines), and 120° and 150° for the anti-Sun direction (black dashed lines).

4.2. Fast Reconstruction of the Fluence

The fast reconstruction method is described in detail elsewhere (Koldobskiy, Kovaltsov, and Usoskin, 2018; Koldobskiy et al., 2019). There, each NM is considered separately, and its count rate increase due to SEPs integrated over the duration of the event is assumed to be directly proportional to the integral SEP fluence exceeding effective rigidity R_{eff}:

$$F(> R_{\mathrm{eff}}) = K_{\mathrm{eff}} \cdot N_{\mathrm{SEP}}, \qquad (5)$$

where K_{eff} is the conversion factor (in cm^{-2}) specific for a given neutron monitor. For the assessment of K_{eff} and R_{eff}, we followed the approach from Koldobskiy et al. (2019) with the factor K defined as follows:

$$K(R, R_c, h) = \frac{F(> R)}{N_{\mathrm{GLE}}} = \frac{\int_R^\infty j(R) dR d\Omega}{\int_{R_c}^\infty j(R) Y(R, h) dR}, \qquad (6)$$

where $j(R)$ is the differential intensity of SEP in the form given in Equation 2 and Y is the NM yield function. We calculated a set of values of K for a wide range of spectral indices γ and steepenings $\delta\gamma$. Then, conversion factor K_{eff} was found as a value with minimal variance of modeled K, while E_{eff} is the energy (converted from the corresponding rigidity R_{eff}), for which that minimal variance of K_{eff} is achieved. Therefore, parameters K_{eff} and E_{eff} (or R_{eff}) depend only on cutoff rigidity R_c and atmospheric depth (altitude) of a given NM location. The integral increase N_{SEP} caused by SEP is defined as

$$N_{\mathrm{SEP}} = \left(\frac{N_{\mathrm{SEP}}^*}{N_{\mathrm{GCR}}^*} \right) \cdot N_{\mathrm{GCR}}, \qquad (7)$$
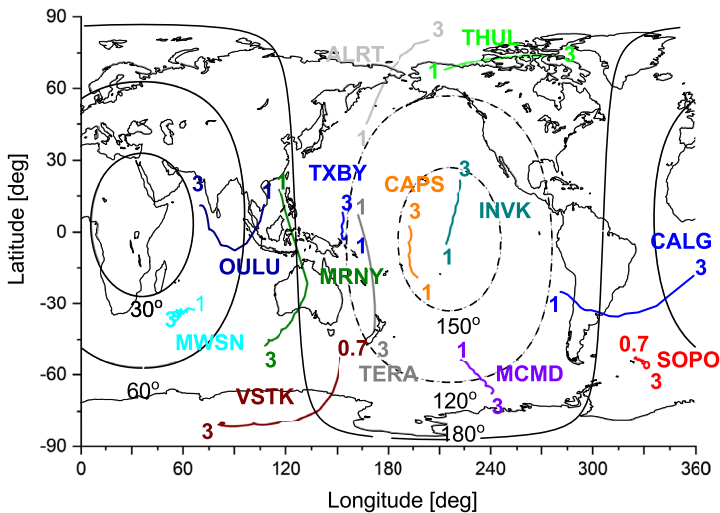
Figure 6 Asymptotic acceptance cones of selected polar NM stations during the sub-GLE on 27 February 1969 at 17:00 UT, shown in geographic coordinates. The cones are indicated as colored lines with NM names next to them and numbers showing the rigidities of SEP (in GV). The contour lines of equal particle pitch angles relative to the derived anisotropy axis are plotted for 30° and 60° for the sunward direction (black solid lines), and 120° and 150° for the anti-Sun direction (black dashed lines).

where ($N^*_{\mathrm{SEP}}/N^*_{\mathrm{GCR}}$) is the ratio of the count rate enhancement due to SEP over the GCR-background count rate observed in the experimental NM data and integrated over the duration of the event. The units of ($N^*_{\mathrm{SEP}}/N^*_{\mathrm{GCR}}$) are %·h. The second term N_{GCR} is the theoretical background count rate of a given NM due to GCR taking into account solar modulation conditions during the event.

     We calculated the values of E_{eff} and K_{eff} for both SOPO and VSTK according to the procedure from Koldobskiy et al. (2019). Theoretical count rates N_{GCR} were estimated using the NM yield function by Mishev et al. (2020), local interstellar spectrum of GCR by Vos and Potgieter (2015) and solar modulation potential ϕ from the data set by Usoskin et al. (2017). Detailed descriptions of the calculation method can be found in Usoskin et al. (2017) and Koldobskiy et al. (2019). The effective energies E_{eff} for stations SOPO and VSTK are both about 700 MeV within the uncertainties. The input data, intermediate results and final SEP fluence values obtained with the fast method are summarized in Table 5. The fluences of the studied sub-GLEs are also plotted in the right-hand panels of Figures 7 and 8. Because of one missing hour in the VSTK data during the sub-GLE on 09 June 1968, the corresponding fluence value $F(> 698\,\mathrm{MeV}) = 2.52 \cdot 10^3$ particles cm^{-2} serves as a lower limit.

     The 95% confidence intervals of the fluence values were calculated with the Monte Carlo approach, similar to Section 4.1. We used 10^4 fluence samples based on K_{eff}, N_{GCR}, and ($N^*_{\mathrm{SEP}}/N^*_{\mathrm{GCR}}$) randomly generated according to their uncertainties shown Table 5. Random samples of N_{GCR} and ($N^*_{\mathrm{SEP}}/N^*_{\mathrm{GCR}}$) had normal distributions, and K_{eff} was distributed uniformly. The uncertainties of E_{eff} and K_{eff} were obtained in the same way as in Koldobskiy et al. (2019), while the uncertainty of the integral increase ($N^*_{\mathrm{SEP}}/N^*_{\mathrm{GCR}}$) was assessed similarly to Usoskin et al. (2020) as a maximum of $0.1 \cdot (N^*_{\mathrm{SEP}}/N^*_{\mathrm{GCR}})$ or 1%·h.

     We note that, unlike the full reconstruction method presented above, the fast method does not account for the anisotropy of SEP fluxes nor it is suited for the reconstruction of the temporal evolution of the particle intensity during the event. However, the robustness

Table 5 Parameters used in the reconstruction of the SEP fluence with the fast method: heliospheric modulation potential ϕ, theoretical background NM count rate N_{GCR}, integral increase due to SEPs (N^*_{SEP}/N^*_{GCR}), effective energy E_{eff}, factor for conversion of the NM increase to fluence K_{eff}. The estimated SEP fluence $F(> E_{eff})$ is also shown. The confidence intervals are 95% (two standard deviations), except for K_{eff} and E_{eff}, which have them as the full ranges. The asterisk * indicates the lower limit because the data were not available for the last hour of the event.

	09 June 1968		27 February 1969	
	SOPO	VSTK	SOPO	VSTK
ϕ (MV)	752	752	756	756
N_{GCR} (counts detector^{-1} s^{-1})	113.5 ± 21.3	173.6 ± 26.4	113.3 ± 21.3	173.2 ± 26.3
(N^*_{SEP}/N^*_{GCR}), (%·h)	2.87 ± 0.58	1.86 ± 0.38	3.89 ± 0.78	5.34 ± 1.06
E_{eff} (MeV)	714^{+66}_{-25}	698^{+57}_{-25}	714^{+66}_{-25}	698^{+57}_{-25}
K_{eff} (cm^{-2})	$0.368^{+0.051}_{-0.075}$	$0.217^{+0.028}_{-0.042}$	$0.368^{+0.051}_{-0.075}$	$0.217^{+0.028}_{-0.042}$
$F(> E_{eff})$ (particles cm^{-2})	$(4.31^{+1.47}_{-1.44}) \cdot 10^3$	$(2.52^{+0.79}_{-0.76}) \cdot 10^3*$	$(5.84^{+2.01}_{-1.94}) \cdot 10^3$	$(7.23^{+2.31}_{-2.21}) \cdot 10^3$

of the proposed method of the integral fluence reconstruction has been demonstrated in application to a list of 58 moderate and strong GLE events (Usoskin et al., 2020), as well as in good agreement with results obtained using the full reconstruction method (Koldobskiy and Mishev, 2022) and direct SEP measurements with the space-borne experiment PAMELA (Bruno et al., 2018; Koldobskiy et al., 2019).

4.3. Fluence from Space-Borne Measurements

Higher-energy SEP fluence values obtained from NM data were complemented with lower-energy ones from space-borne instruments. For that, we took the integral intensity data $J(> 30\,\text{MeV})$ and $J(> 60\,\text{MeV})$ from the OMNI database (Papitashvili and King, 2020), where they are given in units of particles cm^{-2} sr^{-1} s^{-1} with the 1-hour resolution for the studied period. We assumed the angular distribution of SEP as isotropic for relatively low energies 30 and 60 MeV, and thus applied a factor of 4π to obtain the omnidirectional intensity, though the realistic angular distribution of SEPs may not be exactly isotropic.

Fluence $F(> E)$ (in particles cm^{-2}) was calculated as a sum of the hourly-averaged data points over the duration of the event:

$$F(> E) = 4\pi \sum_{i=1}^{n} (J_i(> E) - J_{GCR}(> E)) \cdot \Delta t, \tag{8}$$

where $J_i(> E)$ is the hourly-averaged integral intensity (in particles cm^{-2} sr^{-1} s^{-1}) during the i-th hour of the SEP event, $J_{GCR}(> E)$ is the background integral intensity (in particles cm^{-2} sr^{-1} s^{-1}) due to galactic cosmic rays, calculated as a two-hour mean value before the event, $E = 30$ or $60\,\text{MeV}$, index i corresponds to the hour of the event, and $\Delta t = 1\,\text{hour} = 3600\,\text{s}$ is the time step. The duration of the events on 09 June 1968 and 27 February 1969 marked as n were 44 and 20 hours, respectively, for both energy channels > 30 and $> 60\,\text{MeV}$.

The results of the calculation are shown in Table 6, as well as plotted in Figures 7 and 8 with the label "OMNI".

Table 6 Particle fluence $F(>E)$ during the sub-GLE events on 09 June 1968 and 27 February 1969. Fluence $F(>E)$ is shown in particles cm^{-2}, the confidence intervals are 95% except for E in the fast method, which is given for the full range (see Koldobskiy et al., 2019, for detail). The asterisk * indicates the lower limit because the data were not available for the last hour of the event.

E (MeV)	Method	09 June 1968	27 February 1969
30	OMNI	$9.47 \cdot 10^6$	$5.06 \cdot 10^6$
60	OMNI	$2.57 \cdot 10^6$	$1.83 \cdot 10^6$
500	full	$(2.74^{+0.19}_{-0.09}) \cdot 10^4$	$(5.11^{+0.03}_{-0.07}) \cdot 10^4$
700	full	$(5.35^{+0.37}_{-0.24}) \cdot 10^3$	$(10.7^{+0.11}_{-0.23}) \cdot 10^3$
1000	full	$(6.24^{+0.45}_{-0.37}) \cdot 10^2$	$(13.9^{+0.25}_{-0.48}) \cdot 10^2$
698^{+57}_{-25}	fast	$(2.52^{+0.79}_{-0.76}) \cdot 10^3*$	$(7.23^{+2.31}_{-2.21}) \cdot 10^3$
714^{+66}_{-25}	fast	$(4.31^{+1.47}_{-1.44}) \cdot 10^3$	$(5.84^{+2.01}_{-1.94}) \cdot 10^3$

5. Discussion

The careful examination of the SOPO and VSTK data for the period from May 1964 to December 1969 revealed two new, previously unknown SEP events formally matching the sub-GLE definition (Poluianov et al., 2017). This period contains also six GLE events (Figure 2). Although it is known (e.g., Cliver et al., 2022) that more intense and harder SEP events (associated with GLEs) happen less frequently than moderate ones, more GLEs than sub-GLEs were detected in the studied period. It can be explained by the following: to cause a sub-GLE, the SEP event should be intense enough to induce responses by high-altitude polar NMs, but not more intense than necessary for registration by (near) sea-level polar NMs, when it is classified as GLE. This relatively narrow window in the intensity provides the lower probability of sub-GLEs compared to GLEs.

In this work, we calculated the differential rigidity spectra and integral fluences $F(>E)$ of solar particles during two sub-GLEs. The data are presented in Table 6 and plotted in Figures 7 and 8. The figures show that the data points of $F(>E)$ assessed with three methods (full and fast ones using the NM data, and calculations with OMNI data) are in good agreement with each other for both sub-GLEs. The spectral hardness of the events was also approximately similar, though the sub-GLE on 27 February 1969 is slightly harder than that on 09 June 1968. The fluence of the event in 1969 in the >300 MeV energy range was also higher than that in 1968 due to longer duration (4 hours vs 3 hours) and higher intensity (Table 4).

The values of fluence calculated in this study are compared with earlier estimates based on space-borne measurements presented by Reedy (1977) and Feynman et al. (1990). One can see in Figure 7 that $F(>30\,\text{MeV})$ and $F(>60\,\text{MeV})$ for the event on 09 June 1968, calculated from the OMNI data (magenta triangles) are in good agreement with previous results (black circles and yellow squares). However, there is a notable difference in the event on 27 February 1969 between our work and Feynman et al. (1990). The significantly higher $F(>30\,\text{MeV})$ from the latter source (yellow squares) can be explained by much longer integration time: 5 days including several SEP events in Feynman et al. (1990) vs. 20 hours in this work.

Two new sub-GLE events described here, as well as other sub-GLE events (Mishev, Poluianov, and Usoskin, 2017) show no significant difference to weak GLEs, except for the lower intensity of SEP. We can preliminarily conclude that both sub-GLEs and GLEs are caused by similar SEP events, which can be slightly less intense in the former case than in
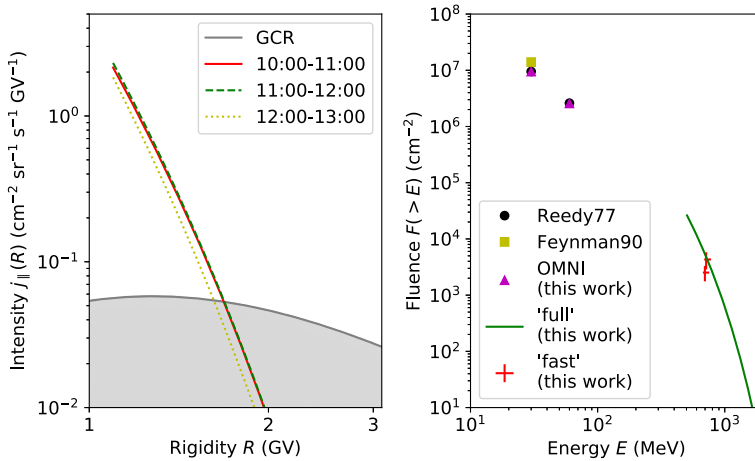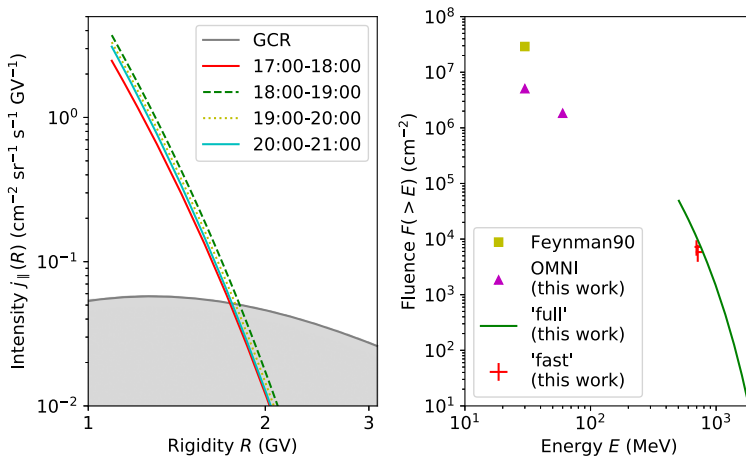
Figure 7   Spectra of intensity $j_\parallel(R)$ for different stages of the event (left panel) and fluence (time- and energy-integrated intensity, right panel) $F(>E)$ estimated for the sub-GLE on 09 June 1968. The time intervals in the left panel are given in UT. The grey line and shaded area indicate the GCR background with the heliospheric modulation ϕ of 752 MV in June 1968 (Usoskin et al., 2017). The data point labels "Reedy77" and "Feynman90" stand for Reedy (1977) and Feynman et al. (1990), respectively.

Figure 8   Spectra of intensity $j_\parallel(P)$ for different stages of the event (left panel) and fluence (time- and energy-integrated intensity, right panel) $F(>E)$ estimated for the sub-GLE on 27 February 1969. The time intervals in the left panel are given in UT. The grey line and shaded area indicate the GCR background with the heliospheric modulation ϕ of 756 MV in February 1969 (Usoskin et al., 2017). The data point $F(>30\text{MeV})$ "Feynman90" (Feynman et al., 1990) is higher than $F(>30\text{MeV})$ "OMNI" from this work because of much longer integration time (5 days).

the latter one. We differentiate sub-GLEs from GLEs in order to maintain the list of standard GLE events consistent in the term of the overall sensitivity of the NM network. A detailed analysis of the sub-GLE spectra and their comparison with the ones of GLEs is still pending.
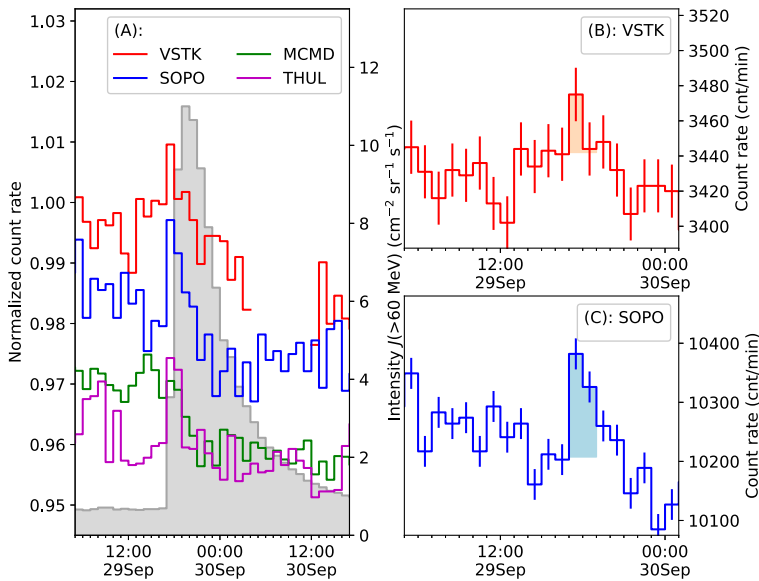
Figure 9 Previously known GLE #18 on 29 September 1968 in the VSTK, SOPO, MCMD and THUL neutron monitor count rates (lines) and proton intensity $J(> 60\,\text{MeV})$ from OMNI (grey shaded area). Panel (A): the NM count rates are shown normalized to the mean of two pre-event hours and with offsets for better visibility (0.00, -0.02, -0.03, -0.04 for VSTK, SOPO, MCMD, and THUL, respectively). Panels (B) and (C): the count rates of VSTK and SOPO, respectively, in units of counts per minute. The shaded areas highlight the increased count rates over the background. The error bars correspond to the 95% confidence intervals (± 2 standard deviations, calculated as square roots of the count rates).

6. Summary

We investigated the period 1964–1969, when two high-altitude polar neutron monitors VSTK and SOPO were simultaneously in operation on the Antarctic Plateau, for possible sub-GLE events. For that purpose, a list of SEP events was compiled using several solar particle event catalogs and data from space-borne instruments available in OMNI (https://omniweb.gsfc.nasa.gov/form/dx1.html). After a careful examination, two events on 09 June 1968 and 27 February 1969 formally matching the sub-GLE definition (Poluianov et al., 2017) were found. Both sub-GLEs showed statistically significant, yet marginal increases in the NM count rates of high-altitude stations VSTK and SOPO, while exhibiting null responses in sea-level neutron monitors THUL and MCMD. The particle fluences for these events were reconstructed using three different methods. The time-integrated SEP fluence spectra $F(> E)$ and the differential intensity $j(R)$ evolving in time for both sub-GLEs are presented.

The sub-GLEs studied in this work are included in the International GLE Database (IGLED, https://gle.oulu.fi).

Appendix

Figure 9 shows the previously known GLE #18 that happened on 29 September 1968, as an illustration of a relatively weak GLE. One can see that the NM count rate profiles are similar to the ones during sub-GLE on 09 June 1968 (Figure 3).

Table 7 The long list of SEP events compiled in this work and used for the search of sub-GLEs. The dash "—" means no significant response in the NM data was found, the asterisk * marks the cases when no VSTK data were available. All GLE events in this table are previously known, but the two sub-GLEs were newly found in this work.

Number	Date	Conclusion	Number	Date	Conclusion
01	1965-Feb-05	—*	20	1968-Sep-29	GLE #18
02	1966-Mar-24	—	21	1968-Oct-04	—*
03	1966-Jul-07	GLE #15	22	1968-Oct-31	—
04	1966-Jul-09	—	23	1968-Nov-01	—
05	1966-Aug-28	—	24	1968-Nov-04	—
06	1966-Sep-02	—	25	1968-Nov-18	GLE #19
07	1966-Sep-14	—	26	1968-Dec-03	—
08	1967-Jan-28	GLE #16	27	1968-Dec-06	—
09	1967-Feb-02	—	28	1969-Feb-25	GLE #20
10	1967-Mar-11	—	29	1969-Feb-26	—
11	1967-May-23	—	30	1969-Feb-27	new sub-GLE
12	1967-May-25	—	31	1969-Feb-28	—
13	1967-May-28	—	32	1969-Mar-30	GLE #21
14	1967-Jun-06	—	33	1969-Apr-11	—
15	1967-Dec-03	—	34	1969-May-13	—
16	1968-Jun-09	new sub-GLE	35	1969-Jun-07	—
17	1968-Jul-06	—	36	1969-Sep-25	—
18	1968-Jul-09	—	37	1969-Sep-27	—
19	1968-Jul-12	—	38	1969-Nov-02	—

Table 8 Mean index K_p used in this work for calculations of the asymptotic acceptance cones and geomagnetic cutoff rigidities of neutron monitors during two sub-GLE events. The data were provided by GFZ German Research Centre for Geosciences (Matzka et al., 2021, https://kp.gfz-potsdam.de/en/).

Date and time (UT)	Mean K_p
sub-GLE on 09 June 1968	
1968-Jun-09 09 – 12 UT	1.33
1968-Jun-09 11 – 12 UT	1.00
sub-GLE on 27 February 1969	
1969-Feb-27 15 – 18 UT	6.33
1969-Feb-27 18 – 21 UT	4.33
1969-Feb-27 21 – 00 UT	3.00

The long list of SEP events, compiled from catalogs and space-borne particle measurements, is presented in Table 7. The list was used to search for sub-GLEs in neutron monitor data using the procedure described in Section 3. It covers the period March 1964 – December 1969, when SOPO, VSTK, THUL and MCMD were in simultaneous operation.

The values of index K_p, which indicates the geomagnetic field disturbance, are shown in Table 8. They were used in calculations of the geomagnetic cutoff rigidities of neutron monitors (Table 1), as well as their asymptotic acceptance cones (Figures 5 and 6). The details of the calculation approach are described in Section 4.1.

Declarations

Competing interests The authors declare no competing interests.

References

Aleksandrov, L.: 1971, The Newton-Kantorovich regularized computing processes. *U.S.S.R. Comput. Math. Math. Phys.* **11**, 46. DOI.

Alken, P., Thébault, E., Beggan, C.D., Amit, H., Aubert, J., Baerenzung, J., Bondar, T.N., Brown, W.J., Califf, S., Chambodut, A., Chulliat, A., Cox, G.A., Finlay, C.C., Fournier, A., Gillet, N., Grayver, A., Hammer, M.D., Holschneider, M., Huder, L., Hulot, G., Jager, T., Kloss, C., Korte, M., Kuang, W., Kuvshinov, A., Langlais, B., Léger, J.-M., Lesur, V., Livermore, P.W., Lowes, F.J., Macmillan, S., Magnes, W., Mandea, M., Marsal, S., Matzka, J., Metman, M.C., Minami, T., Morschhauser, A., Mound, J.E., Nair, M., Nakano, S., Olsen, N., Pavón-Carrasco, F.J., Petrov, V.G., Ropp, G., Rother, M., Sabaka, T.J., Sanchez, S., Saturnino, D., Schnepf, N.R., Shen, X., Stolle, C., Tangborn, A., Tøffner-Clausen, L., Toh, H., Torta, J.M., Varner, J., Vervelidou, F., Vigneron, P., Wardinski, I., Wicht, J., Woods, A., Yang, Y., Zeren, Z., Zhou, B.: 2021, International geomagnetic reference field: the thirteenth generation. *Earth Planets Space* **73**, 49. DOI.

Anastasiadis, A., Lario, D., Papaioannou, A., Kouloumvakos, A., Vourlidas, A.: 2019, Solar energetic particles in the inner heliosphere: status and open questions. *Phil. Trans. Roy. Soc., Math. Phys. Eng. Sci.* **377**, 20180100. DOI.

Barnard, L., Lockwood, M.: 2011, A survey of gradual solar energetic particle events. *J. Geophys. Res. Space Phys.* **116**, A05103. DOI. ADS.

Bazilevskaya, G.A., Makhmutov, V.S., Stozhkov, Y.I., Svirzhevskaya, A.K., Svirzhevsky, N.S.: 2010, Solar proton events recorded in the stratosphere during cosmic ray balloon observations in 1957-2008. *Adv. Space Res.* **45**, 603. DOI. ADS.

Bazilevskaya, G.A., Cliver, E.W., Kovaltsov, G.A., Ling, A.G., Shea, M.A., Smart, D.F., Usoskin, I.G.: 2014, Solar cycle in the heliosphere and cosmic rays. *Space Sci. Rev.* **186**, 409. DOI. ADS.

Bieber, J.W., Evenson, P.: 1995, Spaceship Earth - an optimized network of neutron monitors. In: *Proc. 24th Int. Cosmic Ray Conf.*, *Rome* **4**, 1316,

Bruno, A., Bazilevskaya, G.A., Boezio, M., Christian, E.R., de Nolfo, G.A., Martucci, M., Merge', M., Mikhailov, V.V., Munini, R., Richardson, I.G., Ryan, J.M., Stochaj, S., Adriani, O., Barbarino, G.C., Bellotti, R., Bogomolov, E.A., Bongi, M., Bonvicini, V., Bottai, S., Cafagna, F., Campana, D., Carlson, P., Casolino, M., Castellini, G., Santis, C.D., Felice, V.D., Galper, A.M., Karelin, A.V., Koldashov, S.V., Koldobskiy, S., Krutkov, S.Y., Kvashnin, A.N., Leonov, A., Malakhov, V., Marcelli, L., Mayorov, A.G., Menn, W., Mocchiutti, E., Monaco, A., Mori, N., Osteria, G., Panico, B., Papini, P., Pearce, M., Picozza, P., Ricci, M., Ricciarini, S.B., Simon, M., Sparvoli, R., Spillantini, P., Stozhkov, Y.I., Vacchi, A., Vannuccini, E., Vasilyev, G.I., Voronov, S.A., Yurkin, Y.T., Zampa, G., Zampa, N.: 2018, Solar energetic particle events observed by the PAMELA mission. *Astrophys. J.* **862**, 97. DOI.

Cliver, E.W., Schrijver, C.J., Shibata, K., Usoskin, I.G.: 2022, Extreme solar events. *Living Rev. Solar Phys.* **19**, 2. DOI. ADS.

Cramp, J.L., Duldig, M.L., Flückiger, E.O., Humble, J.E., Shea, M.A., Smart, D.F.: 1997, The October 22, 1989, solar cosmic ray enhancement: an analysis of the anisotropy and spectral characteristics. *J. Geophys. Res.* **102**, 24237. DOI. ADS.

Desai, M., Giacalone, J.: 2016, Large gradual solar energetic particle events. *Living Rev. Solar Phys.* **13**, 3. DOI. ADS.

Desorgher, L., Flückiger, E.O., Gurtner, M., Moser, M.R., Bütikofer, R.: 2005, Atmocosmics: a geant 4 code for computing the interaction of cosmic rays with the Earth's atmosphere. *Int. J. Mod. Phys. A* **20**, 6802. DOI. ADS.

Dodson, H.W., Hedeman, E., Kreplin, R., Martres, M., Obridko, V., Shea, M., Smart, D., Tanaka, H., Švestka, Z., Simon, P.: 1975, Catalog of solar particle events, 1955 – 1969. In: *Catalog of Solar Particle Events 1955 – 1969*, Springer, Berlin, 25.

Environmental Science Services Administration: 1969, Solar-geophysical data number 296. https://www.ngdc.noaa.gov/stp/space-weather/online-publications/stp_sgd/1969/sgd6904.pdf.

Feynman, J., Armstrong, T.P., Dao-Gibner, L., Silverman, S.: 1990, New interplanetary proton fluence model. *J. Spacecr. Rockets* **27**, 403. DOI. ADS.

Golub, G.H., Van Loan, C.F.: 1980, An analysis of the total least squares problem. *SIAM J. Numer. Anal.* **17**, 883.

Hatton, C., Carmichael, H.: 1964, Experimental investigation of the NM-64 neutron monitor. *Can. J. Phys.* **42**, 2443.

King, J.H.: 1974, Solar proton fluences for 1977-1983 space missions. *J. Spacecr. Rockets* **11**, 401.

Kinsey, J.H., McDonald, F.B.: 1968, Observations of the solar proton event of August 28, 1966. In: Kiepenheuer, K.O. (ed.) *Structure and Development of Solar Active Regions* **35**, 536. ADS.

Kocharov, L., Pohjolainen, S., Reiner, M.J., Mishev, A., Wang, H., Usoskin, I., Vainio, R.: 2018, Spatial organization of seven extreme solar energetic particle events. *Astrophys. J. Lett.* **862**, L20. DOI.

Koldobskiy, S., Mishev, A.: 2022, Fluences of solar energetic particles for last three GLE events: comparison of different reconstruction methods. *Adv. Space Res.* **70**, 2585. DOI. ADS.

Koldobskiy, S.A., Kovaltsov, G.A., Usoskin, I.G.: 2018, Effective rigidity of a polar neutron monitor for recording ground-level enhancements. *Solar Phys.* **293**, 110. DOI.

Koldobskiy, S.A., Kovaltsov, G.A., Mishev, A.L., Usoskin, I.G.: 2019, New method of assessment of the integral fluence of solar energetic (> 1 GV rigidity) particles from neutron monitor data. *Solar Phys.* **294**, 94. DOI. ADS.

Kudela, K., Bučik, R., Bobik, P.: 2008, On transmissivity of low energy cosmic rays in disturbed magnetosphere. *Adv. Space Res.* **42**, 1300. DOI.

Larsen, N., Mishev, A., Usoskin, I.: 2023, A new open-source geomagnetosphere propagation tool (OTSO) and its applications. *J. Geophys. Res. Space Phys.* **128**, e2022JA031061. DOI.

Levenberg, K.: 1944, A method for the solution of certain non-linear problems in least squares. *Q. Appl. Math.* **2**, 164.

Lovell, J.L., Duldig, M.L., Humble, J.E., Shea, M.A., Smart, D.F., Flückiger, E.O.: 2002, The cosmic ray ground level enhancement of 6 November 1997. *Adv. Space Res.* **30**, 1045. DOI.

Marquardt, D.: 1963, An algorithm for least-squares estimation of nonlinear parameters. *SIAM J. Appl. Math.* **11**, 431.

Matzka, J., Stolle, C., Yamazaki, Y., Bronkalla, O., Morschhauser, A.: 2021, The geomagnetic Kp index and derived indices of geomagnetic activity. *Space Weather* **19**, e2020SW002641. DOI.

McCracken, K.G., Rao, U.R., Bukata, R.P.: 1967, Cosmic-ray propagation processes: 1. A study of the cosmic-ray flare effect. *J. Geophys. Res.* **72**, 4293. DOI. ADS.

Miroshnichenko, L.: 2015, *Solar Cosmic Rays*, Springer, Cham. ISBN 978-3-319-09428-1. DOI.

Mishev, A., Poluianov, S.: 2021, About the altitude profile of the atmospheric cut-off of cosmic rays: new revised assessment. *Solar Phys.* **296**, 129. DOI.

Mishev, A., Usoskin, I.: 2020, Current status and possible extension of the global neutron monitor network. *J. Space Weather Space Clim.* **10**, 17. DOI.

Mishev, A., Mavrodiev, S., Stamenov, J.: 2005, Gamma rays studies based on atmospheric Cherenkov technique at high mountain altitude. *Int. J. Mod. Phys. A* **20**, 7016. DOI.

Mishev, A., Poluianov, S., Usoskin, I.: 2017, Assessment of spectral and angular characteristics of sub-GLE events using the global neutron monitor network. *J. Space Weather Space Clim.* **7**, A28. DOI.

Mishev, A.L., Koldobskiy, S.A., Kovaltsov, G.A., Gil, A., Usoskin, I.G.: 2020, Updated neutron-monitor yield function: bridging between in situ and ground-based cosmic ray measurements. *J. Geophys. Res. Space Phys.* **125**, e27433. DOI. ADS.

Mishev, A., Usoskin, I., Raukunen, O., Paassilta, M., Valtonen, E., Kocharov, L., Vainio, R.: 2018, First analysis of ground-level enhancement (GLE) 72 on 10 September 2017: spectral and anisotropy characteristics. *Solar Phys.* **293**, 136. DOI. ADS.

Mishev, A.L., Koldobskiy, S.A., Usoskin, I.G., Kocharov, L.G., Kovaltsov, G.A.: 2021, Application of the verified neutron monitor yield function for an extended analysis of the GLE # 71 on 17 May 2012. *Space Weather* **19**, e2020SW002626. DOI.

Mishev, A.L., Kocharov, L.G., Koldobskiy, S.A., Larsen, N., Riihonen, E., Vainio, R., Usoskin, I.G.: 2022, High-resolution spectral and anisotropy characteristics of solar protons during the GLE n°73 on 28 October 2021 derived with neutron-monitor data analysis. *Solar Phys.* **297**, 88. DOI.

Moraal, H., McCracken, K.G.: 2012, The time structure of ground level enhancements in solar cycle 23. *Space Sci. Rev.* **171**, 85. DOI. ADS.

Nevalainen, J., Usoskin, I., Mishev, A.: 2013, Eccentric dipole approximation of the geomagnetic field: application to cosmic ray computations. *Adv. Space Res.* **52**, 22. DOI.

Papitashvili, N.E., King, J.H.: 2020, OMNI hourly data. NASA Space Physics Data Facility. DOI.

Poluianov, S., Batalla, O.: 2022, Cosmic-ray atmospheric cutoff energies of polar neutron monitors. *Adv. Space Res.* **70**(9), 2610.

Poluianov, S.V., Usoskin, I.G., Mishev, A.L., Shea, M.A., Smart, D.F.: 2017, GLE and sub-GLE redefinition in the light of high-altitude polar neutron monitors. *Solar Phys.* **292**, 176. DOI. ADS.

Poluianov, S., Usoskin, I., Mishev, A., Moraal, H., Kruger, H., Casasanta, G., Traversi, R., Udisti, R.: 2015, Mini neutron monitors at Concordia research station, central Antarctica. *J. Astron. Space Sci.* **32**, 281. DOI. ADS.

Reames, D.V.: 2017, *Solar Energetic Particles: A Modern Primer on Understanding Sources, Acceleration and Propagation*, Springer, Heidelberg ISBN 978-3-319-50870-2.

Reames, D.V.: 1999, Particle acceleration at the Sun and in the heliosphere. *Space Sci. Rev.* **90**, 413. DOI.

Reedy, R.: 1977, Solar proton fluxes since 1956. In: *Lunar and Planetary Science Conference Proceedings* **8**, 825.

Shea, M., Smart, D.: 1990, A summary of major solar proton events. *Solar Phys.* **127**, 297.

Shea, M.A., Smart, D.F., Shapley, A.H., Kroehl, H.W.: 1978, Significant solar proton events, 1955-1969, Interim Report Air Force Geophysics Lab., Hanscom AFB, MA. Space Physics Div. ADS.

Simpson, J.A., Fonger, W., Treiman, S.B.: 1953, Cosmic radiation intensity-time variations and their origin. I. Neutron intensity variation method and meteorological factors. *Phys. Rev.* **90**, 934. DOI. ADS.

Smart, D.F., Shea, M.A., Gentile, L.C.: 1994, The relativistic solar proton ground-level enhancements associated with the solar neutron events of 11 June, 15 June 1991. *AIP Conf. Proc.* **294**, 222. DOI.

Tikhonov, A.N., Goncharsky, A.V., Stepanov, V.V., Yagola, A.G.: 1995, *Numerical Methods for Solving Ill-Posed Problems*, Kluwer Academic, Dordrecht ISBN 978-90-481-4583-6.

Tsyganenko, N.A.: 1989, A magnetospheric magnetic field model with a warped tail current sheet. *Planet. Space Sci.* **37**, 5. DOI. ADS.

Usoskin, I.G., Gil, A., Kovaltsov, G.A., Mishev, A.L., Mikhailov, V.V.: 2017, Heliospheric modulation of cosmic rays during the neutron monitor era: calibration using PAMELA data for 2006-2010. *J. Geophys. Res.* **122**, 3875. DOI. ADS.

Usoskin, I., Koldobskiy, S., Kovaltsov, G.A., Gil, A., Usoskina, I., Willamo, T., Ibragimov, A.: 2020, Revised GLE database: fluences of solar energetic particles as measured by the neutron-monitor network since 1956. *Astron. Astrophys.* **640**, A17. DOI.

Väisänen, P., Usoskin, I., Mursula, K.: 2021, Seven decades of neutron monitors (1951-2019): overview and evaluation of data sources. *J. Geophys. Res. Space Phys.* **126**, e28941. DOI. ADS.

Vashenyuk, E.V., Balabin, Y.V., Perez-Peraza, J., Gallegos-Cruz, A., Miroshnichenko, L.I.: 2006, Some features of the sources of relativistic particles at the Sun in the solar cycles 21-23. *Adv. Space Res.* **38**, 411.

Vos, E.E., Potgieter, M.S.: 2015, New modeling of galactic proton modulation during the minimum of solar cycle 23/24. *Astrophys. J.* **815**, 119. DOI. ADS.